



# Back-Integration of Recovered Graphite from Waste-Batteries as Ultra-High Capacity and Stable Anode for Potassium-Ion Battery

Hong Duc Pham,<sup>\*[a, b]</sup> Chinmayee Padwal,<sup>[a, c]</sup> Joseph F. S. Fernando,<sup>[a, b]</sup> Tony Wang,<sup>[a, d]</sup> TaeYoung Kim,<sup>[e]</sup> Dmitri Golberg,<sup>[a, b]</sup> and Deepak P. Dubal<sup>\*[a, b]</sup>

The rapid growth of lithium-ion batteries (LIBs) in many markets from portable electronics to large scale electric vehicles makes it increasingly urgent to address recycling of strategic materials from used batteries. Herein, we report the excellent electrochemical performance of recycled graphite (REG) from spent LIBs, which was successfully employed as an anode in potassium-ion batteries (KIBs). The graphite-anode not only delivers highly reversible capacity of 361.4 mAh g<sup>-1</sup> (at 0.1 C) but also demonstrates good long-term cycling stability. The phase evolution of electrochemically potassium intercalated/deintercalated REG electrodes is elucidated using in-situ X-ray

diffraction. The well-preserved structure of the recycled graphite makes it ideal host for reversible intercalation and deintercalation of K-ions. Furthermore, a potassium-hybrid capacitor was fabricated by coupling the recycled graphite with textile waste-derived activated carbon as cathode material. The cell demonstrates considerable energy density of 84.5 Wh kg<sup>-1</sup> and power density of 400 W kg<sup>-1</sup>, respectively. Apart from the great electrochemical performances, the low-cost, abundant, and sustainable recycled graphite in this work will help to address the challenges in Li-ion battery recycling and show the prospects of next-generation battery system development.

## Introduction

To date, lithium-ion batteries (LIBs) have been intensively utilized in several applications (e.g., electric vehicles, portable tools, and so on) owing to their high energy density and voltage, long lifetime, wide range of operating temperatures, and minimal memory effect.<sup>[1]</sup> Commercial LIBs are successfully used in electric vehicles, fuel cells, portable electronic devices (e.g., tablets, smartphones, laptop) and so forth. A significant increase in consumption of rechargeable batteries puts a high

demand on resources for battery manufacturing and, importantly, creates a larger volume of the battery waste, which poses significant threat to the environment and human health.<sup>[2]</sup> Therefore, minimizing environmental pollution via reusing battery components has gained a considerable interest. To date, numerous studies have focused on the recycling of high-cost cathode materials (e.g., LiCoO<sub>2</sub>, LiFePO<sub>4</sub>, and so on). Conversely, the recovering of anode materials, such as graphite, which are inexpensive and abundant is currently less common.<sup>[3]</sup> Indeed, the cost of graphite is probably lower than that of materials used for cathode materials, but the production and purification of graphite is still rather expensive as well as energy intensive.<sup>[2c]</sup> Therefore, the recycling of graphite from used LIBs is paramount from the resource-recovery point of view.<sup>[4]</sup> In addition, the activated structure of graphite due to electrochemical cycling in LIBs is anticipated to be beneficial for other high-value applications.

Potassium-ion battery (KIB) is an emerging energy storage technology that has a potential to replace existing LIBs due to its low-cost sustainability and similar charge storage kinetics. Carbonaceous materials that contain a graphite-like layered structure have been intensively employed as KIBs anodes since they exhibit a low discharge voltage platform and high energy density. Currently, there are many excellent works on the preparation of high-performance long-cycle carbon materials. The research and development in recent years has been very rapid.<sup>[5]</sup> Among those carbonaceous anodes, graphite has recently been shown to be promising anode material in KIBs. Nevertheless, graphite has recently been shown to be promising anode material in KIBs, it suffers from fast capacity degradation and poor rate capability.<sup>[6]</sup> One of the reasons is gradual distortion of graphite structure during the intercalation

[a] Dr. H. Duc Pham, C. Padwal, Dr. J. F. S. Fernando, Dr. T. Wang,

Prof. D. Golberg, Prof. D. P. Dubal

Centre for Materials Science

Queensland University of Technology

2 George Street, Brisbane 4000, Australia

E-mail: h22.pham@qut.edu.au

deepak.dubal@qut.edu.au

[b] Dr. H. Duc Pham, Dr. J. F. S. Fernando, Prof. D. Golberg, Prof. D. P. Dubal

School of Chemistry and Physics, Faculty of Science

Queensland University of Technology

Brisbane 4000, Australia

[c] C. Padwal

Centre for Agriculture and the Bioeconomy

Queensland University of Technology

Brisbane, QLD 4000, Australia

[d] Dr. T. Wang

Central Analytical Research Facility (CARF)

Queensland University of Technology

Brisbane, QLD 4000, Australia

[e] Prof. T. Kim

Department of Materials Science and Engineering

Gachon University

1342 Seongnam-daero, Sujeong-gu, Seongnam, 13120 South Korea

 Supporting information for this article is available on the WWW under <https://doi.org/10.1002/batt.202100335>

 An invited contribution to a Special Collection dedicated to the 5-Year Anniversary of Batteries & Supercaps.

tion/de-intercalation of  $K^+$  ions due to their larger ionic radius (1.38 Å) as compared to that of  $Li^+$  (0.76 Å), leading to low specific capacity, poor rate-performance and short life.<sup>[7]</sup> Moreover, the long diffusion pathways and the narrow interlayer spacing ( $\sim 0.34$  nm) in graphite results in the large ion diffusion resistance, which makes the insertion of  $K^+$  into graphite more difficult.<sup>[8]</sup> One of the ways to circumvent this issue is to develop an expanded graphitic structure with large interlayer spacings. Recently, few studies have validated this assumption. For instance, Li and co-workers demonstrated that the as-synthesised expanded graphite is beneficial to improve cycling stability and rate capability of KIBs.<sup>[6a]</sup> Additionally, An et al. synthesized an expanded-graphite-based anode, which could reversibly store large size  $K^+$ -ions.<sup>[8]</sup> However, the production of expanded graphite is expensive and requires special syntheses. Therefore, new strategies need to be explored to reliably produce low-cost effectively graphite for KIBs.

In this work, we utilized recycled graphite (REG) from used Li-ion batteries as a sustainable anode for KIBs (Figure 1). According to previous reports, the synthesis of REG requires the chemical and thermal activation processes,<sup>[6a,9]</sup> which might increase the production cost of KIBs. Conversely, in the present work, REG was collected from spent batteries, which not only adds value in the recycled materials but also satisfies the requirements of next-generation battery technology. The electrochemical performance of REG was measured using cyclic voltammetry and galvanostatic charge/discharge techniques. Then, KIHC was constructed using a waste-based activated carbon (AC) as the cathode and REG as the battery-type anode

materials. The cell was tested to evaluate its energy and power densities.

## Experimental Section

### Experimental

The spent LIBs from a laptop were fully discharged in 1 M NaCl for 12 hrs. Consequently, graphite coated with a copper (Cu) foil was collected after the battery was mechanically opened. To loosen the graphite, the Cu foil containing the graphite was immersed in deionised water and sonicated for 2 h. Then, the graphite was cleaned with concentrated HCl (32%) at 50°C for 4 hrs. Prior to centrifuging at 5000 rpm for 5 min, the mixture was continuously sonicated for 2 hrs. Subsequently, the graphite was cleaned by water and dried under vacuum condition. Finally, the cleaned graphite was heat-treated at 800°C for 2 hrs under inert gas to remove residual contaminants. The impurity composition analysis of raw graphite was conducted and showed in Figures S1 and S2.

For the full cell preparation, the blue denim jeans were used as a cathode material. First, they were blended with KOH pellets (1:2 wt % ratio). Subsequently, the addition of deionised water was performed at room temperature. The reaction was kept overnight before the next step.<sup>[10]</sup> Prior to doing the carbonization at 800°C for 1 hr under N<sub>2</sub> atmosphere, the mixture was dried under vacuum condition for overnight. After carbonization, the powder was neutralized with 10% HCl to remove impurities. Afterwards, the powder was repeatedly washed using ethanol and water. Subsequently, it was dried under vacuum condition at 80 °C overnight. The as-prepared material at 800°C was labelled as AC.

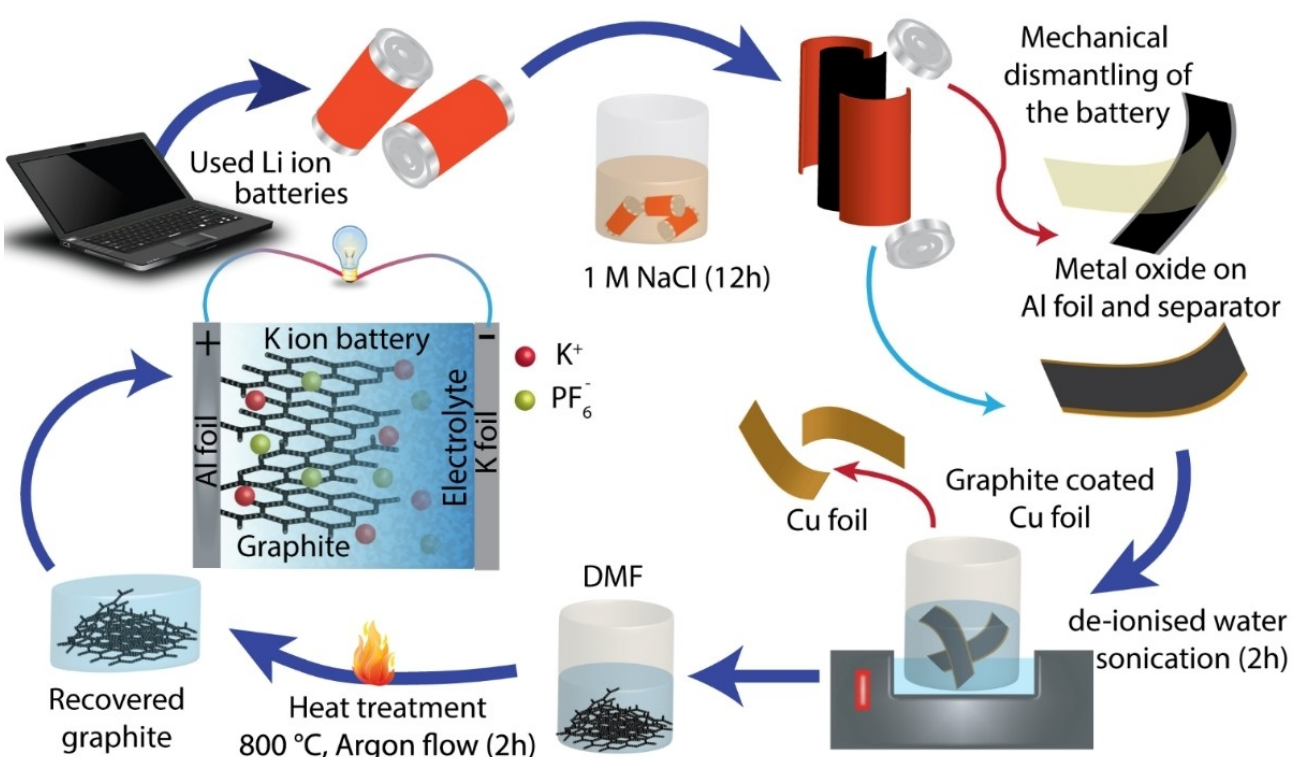


Figure 1. Schematic illustration for recycling of graphite from the spent LIBs and repurposing them as potential electrode materials in next generation KIBs.

## Materials characterization

Phase analysis of the recovered graphite was performed by X-ray diffraction (XRD, Rigaku SmartLab Diffractometer equipped with Cu  $K_{\alpha}$  radiation,  $\lambda = 0.15419$  nm). Phase identification and full pattern fitting were conducted in DIFFRAC.EVA v6 and DIFFRAC.TOPAS v7 respectively. Additionally, X-ray photoelectron spectroscopy (XPS) using a Kratos AXIS Supra spectrometer was performed to provide the chemical nature of the material. The surface morphology and fine structure of the material was characterized on scanning electron microscopy (SEM, JEOL 7001F), transmission electron microscopy (TEM, JEOL 2100), selected area electron diffraction (SAED) patterns, EDX spectra, and high-resolution transmission electron microscopy (HRTEM, JEOL 2100). Raman spectroscopy measurements were carried out using a Renishaw inVia Raman microscope.

## Electrochemical investigation

The electrochemical assessment of graphite in the K-ion battery was performed using a coin-cell configuration (CR2032) which were assembled in an Argon-filled glovebox with oxygen and moisture concentrations kept below 0.1 ppm. For electrode preparation, recycled graphite or textile waste (as active materials), poly(vinylidene fluoride) (as binder) and carbon black (Super P) were mixed at a weight ratio of 80:10:10. Subsequently, the mixture was blended with *N*-methyl-2-pyrrolidone (NMP) solution. Then, the as-prepared material was coated uniformly on an aluminium foil substrate. The paste was dried at 100 °C for 12 hrs in an oven under vacuum condition. For a half-cell configuration of KIBs, while a REG electrode was used as a working electrode, K-foil was employed as the counter electrode. In addition, roughly 150  $\mu$ L electrolyte [1 M potassium hexafluorophosphate (KPF<sub>6</sub>) in ethylene carbonate (EC)/dimethyl carbonate (DMC) (50%:50% v/v)] with a glass microfiber separator were used. The REG anode was performed in a potential window ranging from 0.01 to 2.5 V (vs. K/K<sup>+</sup>) using Neware battery testers. The average mass loaded on aluminium current collector was 1.9 mg cm<sup>-2</sup> for anode and 0.7 mg cm<sup>-2</sup> for cathode. The cyclic voltammetry tests were carried out using a VSP electrochemical workstation (Bio-Logic, VMP-300, France).

Prior to making the full KIHC cells, the REG anode fabricated in a half cell was electrochemically pre-potassiated by cycling few cycles at a current density of 0.1 A g<sup>-1</sup>. Consequently, the REG//AC cells were performed within 0.01–4 V. The total mass loading of both electrodes was maintained at 2.62 mg cm<sup>-2</sup>. Power (*P*) and energy (*E*) were estimated using the following equations:

$$P = \frac{\Delta V \times i}{m}$$

$$E = \frac{P \times t}{3600}$$

$$\Delta V = \frac{E_{\max} + E_{\min}}{2}$$

where *E*<sub>max</sub> and *E*<sub>min</sub> are the maximum and minimum voltages at the discharge (V), *i* is the discharge current (A), *t* is the discharge time (s), and *m* is the mass loading in both anode and cathode (g).

## In-situ X-ray diffraction

REG sample was coated on an aluminium current collector of 15  $\mu$ m thick. The cathode was cut into  $\Phi$ 22 mm size and loaded into an in-situ XRD cell (Beijing Scistar Technology Co., LTD), right

underneath an X-ray transparent 150  $\mu$ m thick beryllium window. The cell was assembled inside an Argon-filled glovebox with KPF<sub>6</sub> electrolyte and potassium metal as the counter electrode. In situ XRD experiments were conducted in a Rigaku SmartLab diffractometer equipped with a Cu Long Fine Focus X-ray tube ( $\lambda = 1.5419$  Å) working at 40 kV and 40 mA. A flat mirror in a CBO- $\alpha$  module was used to remove CuK $\beta$  and bremsstrahlung photons from the primary X-ray beam. Two 5° soller slits were used on both primary and secondary beam paths to limit axial divergence. A 10 mm height limiting slit and a 0.33° incident slit define the illuminated area on the graphite anode layer. A Hypix3000 detector was operated in 1D mode collecting 3.82° 2θ diffraction data simultaneously. The height of the in-situ cell was accurately aligned according to the Al 220 peak position from the aluminium current collector. A knife edge was placed 3 mm above the beryllium window surface to block low angle air-scattering background. A total of 170 XRD patterns were collected during the first two (dis)charge cycles of the KIB. Each pattern was scanned for 10 min from 10–70° 2θ range with a step size 0.04° 2θ. The battery was cycled between 0.02–2.50 V at a specific current of 30 mAg<sup>-1</sup> utilizing the Gamry Interface 1010E potentiostat.

## Results and Discussion

### Recycled graphite (REG) anode

The structural and compositional properties of a battery REG sample were studied using Raman and XPS analyses (Figure 2). As displayed in Figure 2(a), the Raman spectrum exhibited typical D and G bands that are appeared at around 1355 and 1583 cm<sup>-1</sup>, respectively, corresponding to a carbon material.<sup>[6a]</sup> Moreover, the G band corresponds to the graphitic domains consisting of sp<sup>2</sup> carbon atoms while the D band represents the disordered carbon arrangement. The I<sub>D</sub>/I<sub>G</sub> intensity ratio was used to estimate the degree of disorder of the material.<sup>[9]</sup> Herein, the ratio was found to be 0.41, indicating the low graphitization degree of REG.<sup>[3,8]</sup> Additionally, the presence of a 2D peak at around 2705 cm<sup>-1</sup> indicated the existence of a graphitic structure in the recovered material.<sup>[3]</sup> XRD was carried out to confirm the crystal structure of REG material. The XRD pattern (see Figure 2b) well matched a hexagonal phase of graphite (PDF# 00-041-1487, Graphite-2H, space group: P63/mmc), where peaks at 26.6° and 55° are to be attributed to the (002) and (004) lattice planes of graphite, respectively. The peaks seen at 42.3° and 44.4° are matched to the (100) and (101) planes, respectively.<sup>[9]</sup> The d<sub>002</sub> measured from this pattern is 0.3365 nm. A practical estimation for degree of graphitization is the ratio of (3.44-d<sub>002</sub>)/(3.44–3.354),<sup>[11]</sup> which was calculated to be 87% from the XRD pattern (Figure 2b). XPS measurements were performed to further confirm the elemental composition in the recycled graphite. The full survey spectrum of the REG divulged two main characteristic peaks at 284 and 533 eV, corresponding to the carbon (C1s) and oxygen (O1s), respectively (Figure S3). Meanwhile, other elements were not observed, suggesting the absence of any impurity in REG. Figure 2(c) shows the deconvoluted high resolution C 1s XPS spectrum. The component at 284.0 eV was attributed to sp<sup>2</sup> carbon of REG sample, while the peak at 284.9 eV is a fingerprint of sp<sup>3</sup> carbon. Additionally, the peaks at 285.9 and

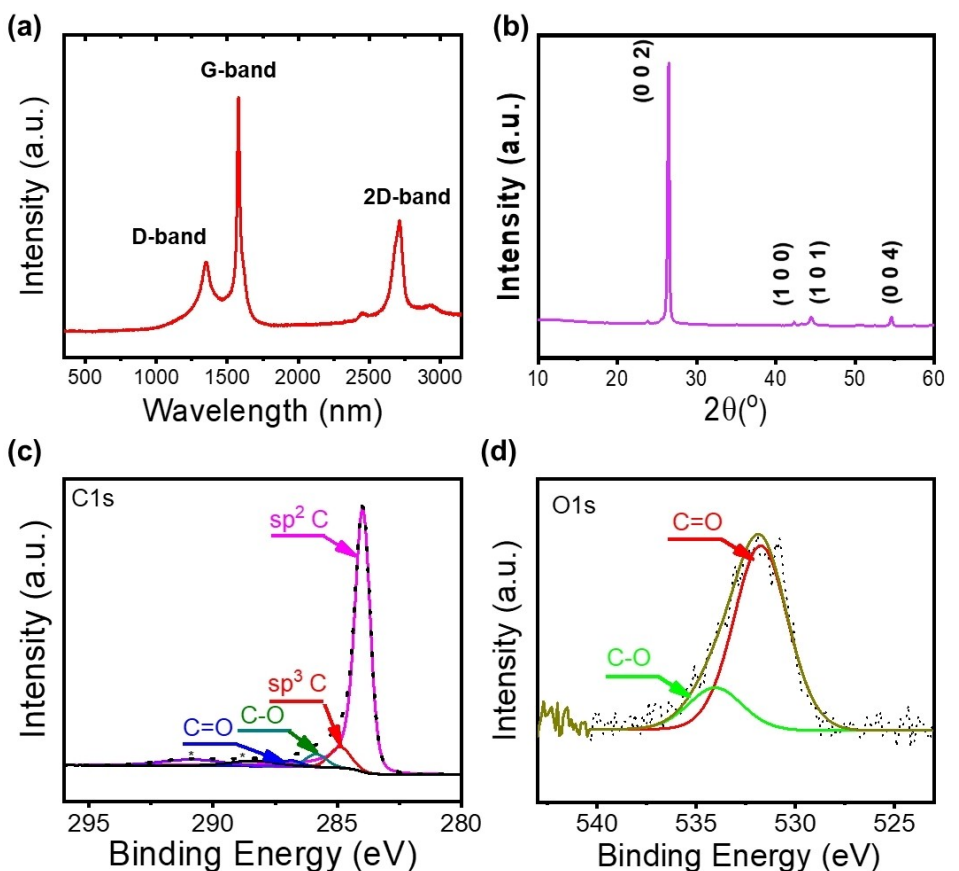


**Figure 2.** a) Raman spectrum, b) XRD pattern, and c, d) high-magnified XPS spectrum for C1s and O1s collected from the REG.

287.0 eV were attributed to C—O and C=O groups, respectively. Moreover, two broad peaks observed at 288.5 and 291.0 eV correspond to plasmon loss features of a  $\text{sp}^2$  carbon.<sup>[10]</sup> Figure 2(d) shows the high-resolution O 1s XPS spectrum obtained from REG sample, which was deconvoluted into two components. The peaks at 531.7 and 533.9 eV were attributed to C=O and C—O bonds, respectively.

FESEM and HRTEM images (Figure 3) were acquired to understand the fine structure of recovered REG samples. The FESEM image (Figure 3a) shows a flake-like morphology. TEM image (Figure 3b) displays a thin flake of REG revealing its fine layered structure. Figure 3(c) shows a HRTEM image acquired from the region marked in Figure 2b. While the d-spacing of typical commercial graphite is roughly of 0.335 nm,<sup>[12]</sup> that of REG samples ranges from 0.34 to 0.36 nm (Figure 3c), indicating the relatively expanded interlayer spacing due to long-term (de)intercalation of Li. The SAED pattern (Figure 3d, acquired from the marked region in 3b) agrees well with XRD data, and indicates the presence of (002), (101) and (110) planes of graphite. STEM-EDX analysis was performed to verify the purity of the sample. STEM-EDX mapping (Figure 3e) and the corresponding EDX spectrum (Figure S4) clearly show that cleaning procedure was successful, and the sample is free from impurities (Note: Cu  $K_{\alpha}$  signal is due to the TEM grid).

The potassium storage behavior of the REG anode is first tested in half-cell configuration. The electrochemical perform-

ances of graphite as KIB anodes in  $\text{KPF}_6$ -EC/DMC electrolyte are shown in Figures 4 and S5. Figure S5 exhibits cyclic voltammetry (CV) curves measured in a potential window of 0.01–2.5 V (vs.  $\text{K}/\text{K}^+$ ) at a scan rate of 0.1 mV s<sup>-1</sup>. During the first two scans, the CV curves have the similar shape to that of commercial graphite as reported previously.<sup>[13]</sup> The first five galvanostatic charge/discharge (GCD) cycles at a current density of 0.1 C (where 1 C = 279 mA g<sup>-1</sup>) is illustrated in Figure 4a. The initial discharge and charge capacities are 612 and 319 mA h g<sup>-1</sup>, respectively. As shown in the first discharge, the sudden drop in the initial capacity is attributed to the electrolyte decomposition and formation of SEI layers, which are normally observed in graphite-based anodes of KIBs. Consequently, a small plateau at around 0.48 V and a slope thereafter to 0.01 V were observed which may be associated with potassiation and depotassiation reactions between graphitic layers and a porous structure of carbon materials.<sup>[14]</sup>

The galvanostatic charge/discharge profiles of the REG anodes at different rates are recorded and illustrated in Figure 4b. The reversible specific capacities are estimated to be 382 mA h g<sup>-1</sup> at 0.1 C and 148 mA h g<sup>-1</sup> at 1 C, which indicates that the REG electrode exhibits excellent structural stability and shows a great cycling stability at higher rates. The nominal working voltage is found to be 0.33 V (vs. K). The rate capability of the RGP cell at various current rates is also evaluated as shown in Figure 4c. It delivers a specific capacity of 361.4,

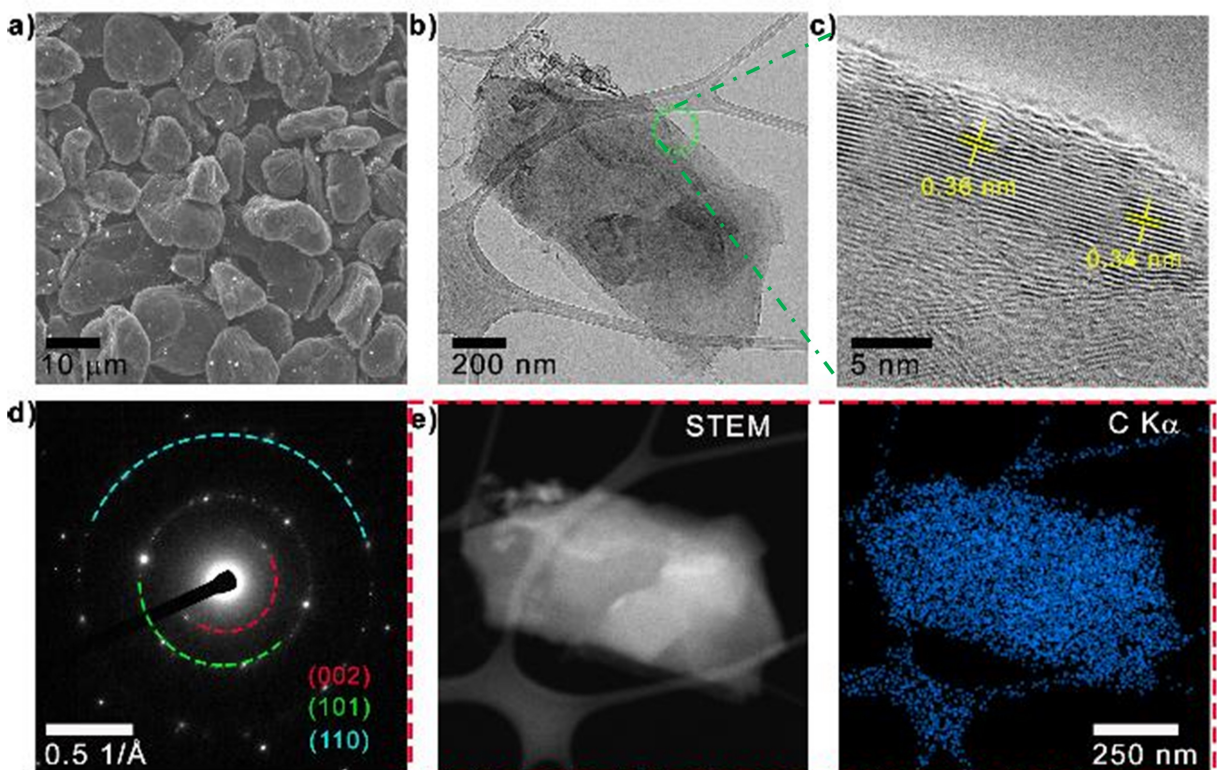


**Figure 3.** a) SEM image of recycled graphite. b) TEM image of recycled graphite. c) High resolution TEM image displaying a layered structure. d) SAED pattern. e, f) STEM image and EDX elemental map for REG.

300.4, 257.6, 212.5, 175.2, 154.6, 66.9, 26.4, and 13.8 mAh g<sup>-1</sup> at the current densities of 0.1 C, 0.2 C, 0.4 C, 0.6 C, 0.8 C, 1 C, 2 C and 4 C, respectively. Over the entire discharge-charge process, when the current density turns to 0.2 C, the capacity of the electrodes recovers to 269.3 mAh g<sup>-1</sup>, suggesting the excellent rate capability. Furthermore, the cycling stability of REG anode was recorded at 0.4 C over 250 cycles, as illustrated in Figure 4d. Interestingly, while retaining 70% of the initial capacitance, the REG anode shows almost 100% Coulombic efficiency.

Figure 4e displays a comparison of the specific capacity of the REG anode for KIB with other best earlier attempts using carbon-based anodes for KIBs.<sup>[6,8,15]</sup> As it can be seen, the capacity of the present REG anode-based devices is on top of such comparison because: 1) the extended graphite electrode was still not cracking;<sup>[8]</sup> 2) the enlarged graphitic structure of REG electrode was well maintained, which resulted in the facile potassiation/depotassiation process at varied current densities.<sup>[6a]</sup>

Compared to ex-situ XRD measurement, in-situ XRD measurement has unrivalled advantages in probing the interlayer spacing changes of REG under K<sup>+</sup> ions (de)intercalation. A few obstacles (e.g., crystallization of KPF<sub>6</sub> electrolyte, carbonisation of K<sup>+</sup> ions, reaction with air and moisture etc.) can be totally avoided. The in-situ XRD patterns in the 15°–35° 2θ (Cu K<sub>α</sub>) angular range revealing the graphene interlayer changes are aligned with the voltage evolutions as well as the stoichiometric number × of K<sup>+</sup> ion in the K<sub>x</sub>C<sub>8</sub> formula in Figure 5a. During

the first discharge, the graphite 002 diffraction peak at 26.6° initially splits into two peaks, which further shift to lower and higher angles due to gradual K<sup>+</sup> intercalation. The peak shifts are not continuous but show two obvious steps around 2.8 × 10<sup>4</sup> and 4 × 10<sup>4</sup> s till fully discharge. The fully discharged peaks align with KC<sub>8</sub> (PDF 01-073-9679). The peaks reverse back along same steps to the initial graphite position after charging. These steps of graphite phase changes due to K<sup>+</sup> ion intercalation have been reported as graphite → stage 4 → stage 2 → stage 1 for KIBs made from commercial graphite, in which the stage numbers "n" are defined as the number of graphene layers in between two intercalated K<sup>+</sup> ion layers.<sup>[16]</sup> Based on the current in situ XRD result, the K<sup>+</sup> ion intercalation mechanism of REG exhibits same behaviour as the commercial graphite. The two split peaks were explained as 00n and 00(n+1) reflections of the K<sup>+</sup> ion intercalated graphite compound. Equations (2)–(4) mentioned in the earlier attempt<sup>[16]</sup> can be combined as below:

$$d_{00n} = \frac{d_i + d_0(n-1)}{n}, \quad d_{00(n+1)} = \frac{d_i + d_0(n-1)}{n+1}, \quad (1)$$

where "d<sub>i</sub>" stands for the K<sup>+</sup> intercalated interlayer spacing, "d<sub>0</sub>" stands for the empty interlayer spacing, "n" the average number of graphene layers in between two K<sup>+</sup> intercalated layers.

The stoichiometry numbers × in the K<sub>x</sub>C<sub>8</sub> formula are linked to d-spacings defined in Equation (1) through its reverse propor-

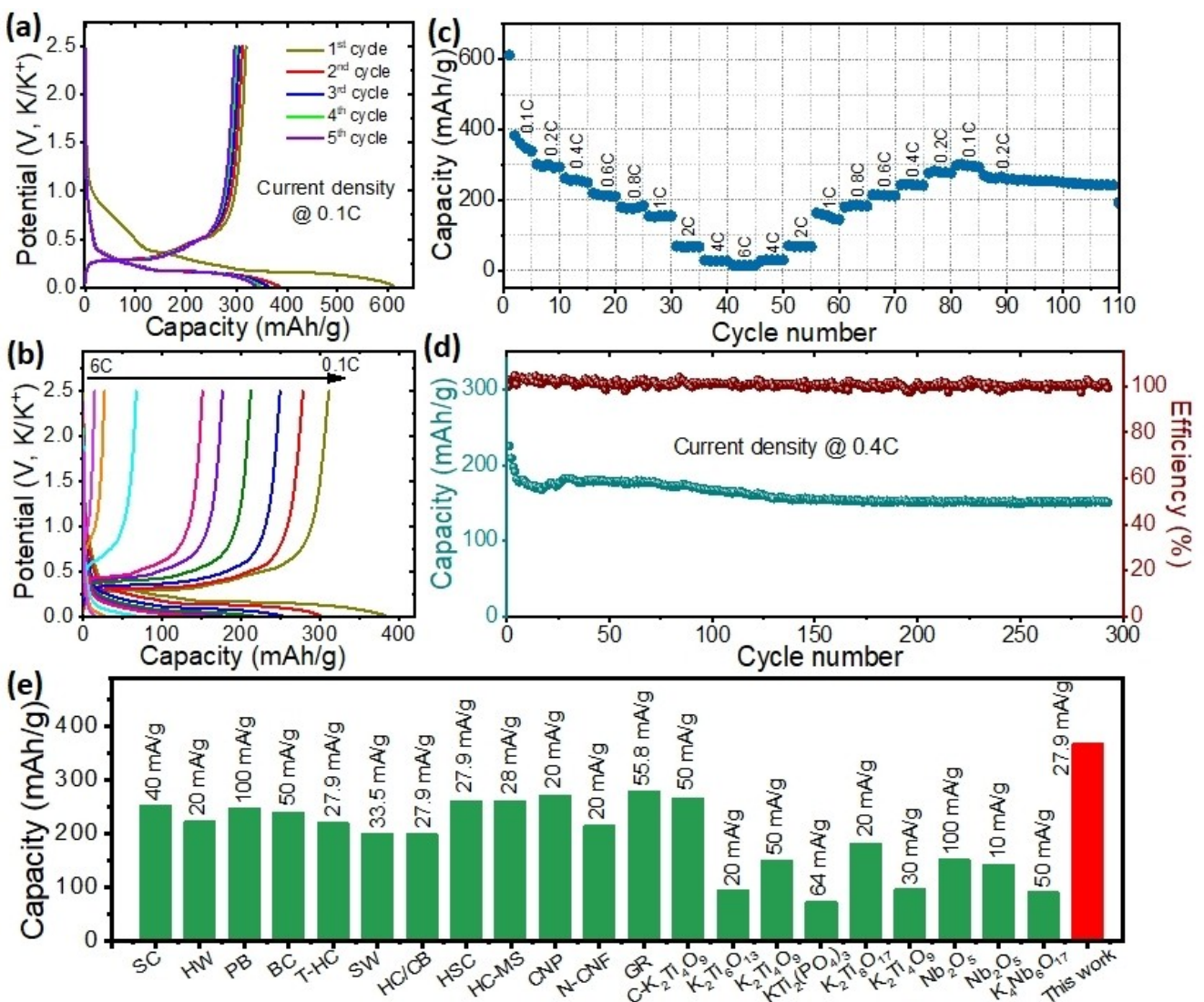


**Figure 4.** Electrochemical performances of the REG anode material in the K-ion half cell: a) Initial galvanostatic charge/discharge (GCD) curves recorded at 0.1 C ( $1\text{C} = 279 \text{ mAh g}^{-1}$ ). b) GCD curves recorded at different current densities. c) Rate-performance of the REG electrode. d) Long-term cycling stability with corresponding Coulombic efficiency over 290 cycles at 0.4 C. e) Comparison of specific capacity of half cells with different carbon-based anode materials recorded at respective current densities (SC: Skimmed cotton, PB: Potato-biomass, BC: Bacterial cellulose, T-HC: tire-waste, SW: Seafood waste, HC/CB: Hard carbon/Carbon black, HSC: Hard-soft composite carbon, WS: walnut septum, MEG: Mildly-expanded graphite, CEGR: commercial expanded graphite, GR: Graphite).

tional relationship with the “stage number  $n$ ”. This explanation was successfully verified by modelling Equation (1) in DIFFRAC-TOPAS v7 software to fit all the in-situ XRD patterns (Figure 5b). The value of  $\alpha$  can be directly refined from the changes of the two split peak positions and aligned on the right side of Figure 5a.

#### Full K-ion hybrid capacitor (KIHC) with REG anode//AC cathode

Based on the outstanding electrochemical features of the battery recycled graphite in a half cell, a KIHC, including REG as an anode and activated carbon (AC) as a cathode, was assembled. The CV behavior observed for the REG//AC KIHC at

scan rates ranging from 0.5 to 6  $\text{mVs}^{-1}$  with a voltage range from 0.01 to 4 V are shown in Figure S6. All CV curves display quasi-rectangular shapes without obvious redox peaks, confirming the contribution from the capacitance mechanism. Figure 6a illustrates the galvanostatic charge-discharge profiles ranging from 0.01 to 0.2  $\text{Ag}^{-1}$ , which are symmetric in nature and follow the capacitive trend. The energy and power densities of REG//AC were evaluated based on the mass loading in both electrodes. The maximum energy density was achieved at  $84.5 \text{ Wh kg}^{-1}$  at a power density output of  $400 \text{ W kg}^{-1}$ . Notably, the KIHC shows the long-term cyclability with almost 100% Coulombic efficiency and minimal loss when measured at  $0.04 \text{ Ag}^{-1}$  after 1000 cycles (Figure 6b). To illustrate the high-energy and high-power features, a comparison of the energy and power densities of current KIHCs was made

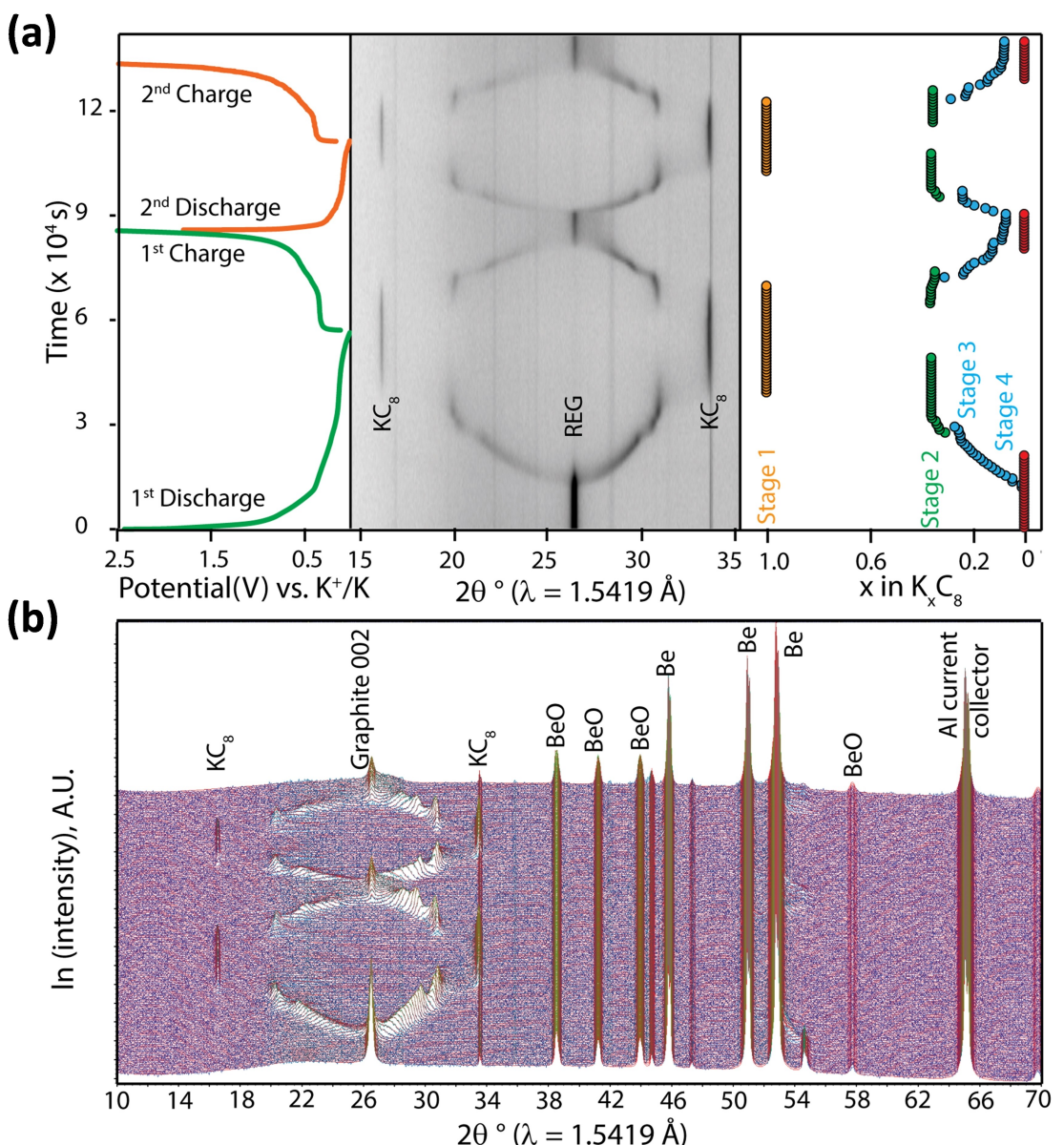


**Figure 5.** In situ XRD patterns of REG during the first two cycles in the voltage range of between 0.02–2.5 V at 0.1 C: a) Voltage changes aligned with the interlayer spacing changes monitored by selected  $2\theta$  range (middle), from which the stichometry number  $x$  of the  $K_xC_8$  formula was refined (right); b) full pattern fittings of in-situ XRD data using Equation (1) in DIFFRAC.TOPAS v7.

(Figure 6c). Compared with the resultant device in the Ragone plot of other earlier attempts, such as N-CNTs//LSG,<sup>[14]</sup> NGC// $K_2Ti_6O_{13}$ ,<sup>[17]</sup> AC//graphite,<sup>[18]</sup> and  $K_2TP$ //AC,<sup>[19]</sup> the present KHIC displays better electrochemical performance.

## Conclusions

We have successfully demonstrated the use of a low-cost anode material derived from recovered graphite in spent LIBs for sustainable K-ion batteries, providing a novel approach of recycling. The extended interlayer distance and well-preserved graphitic structure of REG were confirmed using several material characterization techniques. Benefiting from the well-

maintained structure, the REG showed high reversible capacity of  $361.4 \text{ mAh g}^{-1}$  when employed as an anode material in KIB. Additionally, good long-term cycle stability was recorded at 0.4 C for over 290 cycles, further confirming the structural stability of the REG. Notably, the mechanism of potassium ion intercalation and deintercalation staging in REG electrodes was elucidated. An as-assembled KIHC delivered an energy and power density of  $84.5 \text{ Wh kg}^{-1}$  and  $400 \text{ W kg}^{-1}$ , respectively, with remarkable cycling stability. The results will help to address the challenges in recycling technologies and add values for repurposing applications.

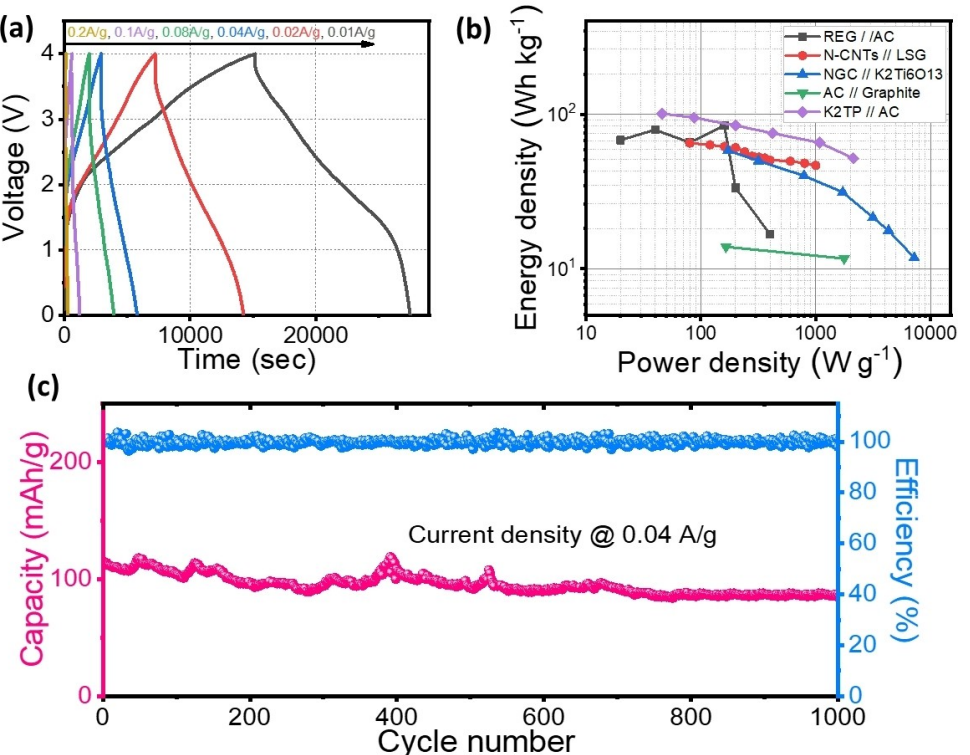


**Figure 6.** Electrochemical properties of a REG//AC full cell: a) Galvanostatic charge/discharge curves recorded at different applied current densities. b) Long cyclic stability of the REG//AC cell tested at current density of 0.04 A g<sup>-1</sup> over 1000 cycles. c) Ragone plot with specific energy and power values calculated by the total active mass in both cathode and anode.

## Acknowledgements

The authors acknowledge the facilities, and the scientific and technical assistance of staff at Central Analytical Research Facility (CARF), Queensland University of Technology (QUT). D.P.D. acknowledges QUT's start-up grant: 323000-0424/07. H.D.P. and D.P.D. would like to acknowledge the Post-Doc Fellowship sponsored by the Centre for Materials Science, QUT, Australia. D.G. and J.F.S.F. are grateful to the Australian Research Council (ARC) for funding in the frame of a Laureate Fellowship FL160100089 and QUT Projects No. 323000-0355/51 and 323000-0348/07.

## Conflict of Interest

The authors declare no conflict of interest.

## Data Availability Statement

Research data are not shared.

**Keywords:** battery recycling · in-situ XRD · potassium-ion battery · recycled graphite

- [1] T. H. Anh Nguyen, S. Y. Oh, *Waste Manage.* **2020**, *120*, 755–761.
- [2] a) D. J. Garole, R. Hossain, V. J. Garole, V. Sahajwalla, J. Nerkar, D. P. Dubal, *ChemSusChem* **2020**, *13*, 3079–3100; b) C. M. Costa, J. C. Barbosa, R. Gonçalves, H. Castro, F. J. D. Campo, S. Lanceros-Méndez, *Energy Storage Mater.* **2021**, *37*, 433–465; c) E. Fan, L. Li, Z. Wang, J. Lin, Y. Huang, Y. Yao, R. Chen, F. Wu, *Chem. Rev.* **2020**, *120*, 7020–7063.
- [3] H. D. Pham, M. Horn, J. F. S. Fernando, R. Patil, M. Phadatare, D. Golberg, H. Olin, D. P. Dubal, *Sustain. Mater. Technol.* **2020**, *26*, e00230.
- [4] S. Rothermel, M. Evertz, J. Kasnatscheew, X. Qi, M. Grutzke, M. Winter, S. Nowak, *ChemSusChem* **2016**, *9*, 3473–3484.
- [5] a) H. Ding, J. Zhou, A. M. Rao, B. Lu, *Natl. Sci. Rev.* **2021**, *8*, nwaa276; b) L. Fan, Y. Hu, A. M. Rao, J. Zhou, Z. Hou, C. Wang, B. Lu, *Small Methods* **2021**, *5*(12), 2101131; c) C.-B. Sun, Y.-W. Zhong, W.-J. Fu, Z.-Q. Zhao, J. Liu, J. Ding, X.-P. Han, Y.-D. Deng, W.-B. Hu, C. Zhong, *Tungsten* **2020**, *2*, 109–133, <https://link.springer.com/article/10.1007/s42864-020-00038-6>; d) J. Wang, H. Wang, X. Zang, D. Zhai, F. Kang, *Batteries & Supercaps* **2021**, *4*, 554–570; e) B. Xu, S. Qi, F. Li, X. Peng, J. Cai, J. Liang, J. Ma, *Chin. Chem. Lett.* **2020**, *31*, 217–222.
- [6] a) X. Li, Y. Lei, L. Qin, D. Han, H. Wang, D. Zhai, B. Li, F. Kang, *Carbon* **2021**, *172*, 200–206; b) Z. Jian, W. Luo, X. Ji, *J. Am. Chem. Soc.* **2015**, *137*, 11566–11569.
- [7] a) Y. Wu, H. Zhao, Z. Wu, L. Yue, J. Liang, Q. Liu, Y. Luo, S. Gao, S. Lu, G. Chen, X. Shi, B. Zhong, X. Guo, X. Sun, *Energy Storage Mater.* **2021**, *34*, 483–507; b) Y. Wu, Y. Sun, J. Zheng, J. Rong, H. Li, L. Niu, *Chem. Eng. J.* **2021**, *404*, 126565, <https://www.sciencedirect.com/science/article/pii/S1385894720326930>; c) H. D. Pham, K. Mahale, T. M. L. Hoang, S. G. Mundree, P. Gomez-Romero, D. P. Dubal, *ACS Appl. Mater. Interfaces* **2020**, *12*, 48518–48525.
- [8] Y. An, H. Fei, G. Zeng, L. Ci, B. Xi, S. Xiong, J. Feng, *J. Power Sources* **2018**, *378*, 66–72.
- [9] Z. Tai, Q. Zhang, Y. Liu, H. Liu, S. Dou, *Carbon* **2017**, *123*, 54–61.
- [10] H. D. Pham, J. F. S. Fernando, M. Horn, J. MacLeod, N. Motta, B. Doherty, A. Payne, A. K. Nanjundan, D. Golberg, D. Dubal, *Electrochim. Acta* **2021**, *389*, 138717.
- [11] a) D. Hou, K. Li, R. Ma, Q. Liu, *J. Materomics* **2020**, *6*, 628–641; b) G. P. K. Ch. N Barnakov, A. N. Popova, S. A. Sozinov, Z. R. Ismagilov, *Eurasian Chem.-Technol. J.* **2015**, *17*, 87–93.

- [12] B. Vadlamani, K. An, M. Jagannathan, K. S. R. Chandran, *J. Electrochem. Soc.* **2014**, *161*, A1731–A1741.
- [13] L. Wang, J. Yang, J. Li, T. Chen, S. Chen, Z. Wu, J. Qiu, B. Wang, P. Gao, X. Niu, H. Li, *J. Power Sources* **2019**, *409*, 24–30.
- [14] M. Moussa, S. A. Al-Bataineh, D. Losic, D. P. Dubal, *Appl. Mater. Res.* **2019**, *16*, 425–434.
- [15] a) C. Gao, Q. Wang, S. Luo, Z. Wang, Y. Zhang, Y. Liu, A. Hao, R. Guo, *J. Power Sources* **2019**, *415*, 165–171; b) W. Cao, E. Zhang, J. Wang, Z. Liu, J. Ge, X. Yu, H. Yang, B. Lu, *Electrochim. Acta* **2019**, *293*, 364–370; c) H. Li, Z. Cheng, Q. Zhang, A. Natan, Y. Yang, D. Cao, H. Zhu, *Nano Lett.* **2018**, *18*, 7407–7413; d) X. He, J. Liao, Z. Tang, L. Xiao, X. Ding, Q. Hu, Z. Wen, C. Chen, *J. Power Sources* **2018**, *396*, 533–541; e) Y. Li, R. A. Adams, A. Arora, V. g. Pol, A. M. Levine, R. J. Lee, K. Akato, A. K. Naskar, M. P. Paranthaman, *J. Electrochem. Soc.* **2017**, *164*, A1234–A1238; f) Z. Jian, S. Hwang, Z. Li, A. S. Hernandez, X. Wang, Z. Xing, D. Su, X. Ji, *Adv. Funct. Mater.* **2017**, *27*, 1700324; g) C. Chen, Z. Wang, B. Zhang, L. Miao, J. Cai, L. Peng, Y. Huang, J. Jiang, Y. Huang, L. Zhang, J. Xie, *Energy Storage Mater.* **2017**, *8*, 161–168; h) C. Vaalma, G. A. Giffin, D. Buchholz, S. Passerini, *J. Electrochem. Soc.* **2016**, *163*, A1295–A1299.
- [16] H. Onuma, K. Kubota, S. Muratsubaki, W. Ota, M. Shishkin, H. Sato, K. Yamashita, S. Yasuno, S. Komaba, *J. Mater. Chem. A* **2021**, *9*, 11187–11200.
- [17] S. Dong, Z. Li, Z. Xing, X. Wu, X. Ji, X. Zhang, *ACS Appl. Mater. Interfaces* **2018**, *10*, 15542–15547.
- [18] A. Le Comte, Y. Reynier, C. Vincens, C. Leys, P. Azaïs, *J. Power Sources* **2017**, *363*, 34–43.
- [19] Y. Luo, L. Liu, K. Lei, J. Shi, G. Xu, F. Li, J. Chen, *Chem. Sci.* **2019**, *10*, 2048–2052.

Manuscript received: November 8, 2021

Revised manuscript received: December 5, 2021

Accepted manuscript online: December 13, 2021

Version of record online: December 27, 2021